

# Uncertainties in the S-Z selected cluster angular power spectrum

J. D. Cohn<sup>1</sup>, Kenji Kadota<sup>2,3</sup>

<sup>1</sup> *Space Sciences Lab and Theoretical Astrophysics Center,* <sup>2</sup> *Department of Physics,*  
*University of California, Berkeley, CA 94720, USA*

<sup>3</sup> *NASA/Fermilab Astrophysics Center, Fermi National Accelerator Laboratory, Batavia, IL 60510*  
email: jcohn@astron.berkeley.edu, kadota@fnal.gov

## ABSTRACT

Large SZ selected galaxy cluster surveys are beginning imminently. We compare the dependence of the galaxy cluster angular power spectrum on different modeling assumptions and quantify the tradeoff between depth and area of surveys for its measurement. We also identify the scaling behavior of the cluster angular power spectrum with respect to  $\sigma_8$ .

*Subject headings:* cosmic microwave background—cosmological parameters—galaxies: clusters: general

## 1. Introduction

The Sunyaev Zel'dovich (hereafter SZ) effect is the upscattering of cosmic microwave background photons by the hot electrons in galaxy clusters (Sunyaev & Zel'dovich (1972; 1980)). As the surface brightness of a cluster in the SZ is redshift independent, and the signal is relatively insensitive to the poorly known cluster core structure, the SZ effect is a powerful tool to select and study galaxy clusters. The field of SZ measurements has progressed rapidly from a handful of SZ detections for already-known galaxy clusters to SZ maps of several clusters to the current stage: cluster surveys designed exclusively for SZ detection. For reviews, see for example Birkinshaw (1999) and Carlstrom, Holder & Reese (2002). Some surveys are already in progress such as ACBAR<sup>1</sup> and SZA<sup>2</sup>. Others are on the verge of taking data, such as AMI<sup>3</sup> and APEX<sup>4</sup>, and ACT<sup>5</sup> expects to be ready the end of 2006. For instance, APEX, starting observation next year, is expected to observe thousands of previously unknown clusters. Future surveys, taking place within the next decade,

---

<sup>1</sup><http://astronomy.sussex.ac.uk/~romer/research/blind.html>

<sup>2</sup><http://astro.uchicago.edu/sza/overview.html>

<sup>3</sup><http://www.mrao.cam.ac.uk/telescopes/ami/index.html>

<sup>4</sup><http://bolo.berkeley.edu/apexsz/index.html>

<sup>5</sup><http://www.hep.upenn.edu/~angelica/act/act.html>

can be expected to observe an order of magnitude more clusters, for instance SPT<sup>6</sup>, and Planck<sup>7</sup>. For a full list of current and upcoming experiments, see for example the CMB experiment page at LAMBDA<sup>8</sup>.

The prospect of combining these theoretical predictions and observational data on galaxy clusters to constrain fundamental cosmological parameters has led to much excitement (e.g. Holder, Haiman & Mohr (2001), Majumdar & Mohr (2002) and references below). With large survey data on the horizon, and the detailed design of later experiments taking shape, it is timely to identify which theoretical assumptions are the most crucial to pin down in order to use the science harvest from these experiments. The initial galaxy cluster information these surveys will produce will be number counts and the angular correlation function/cluster power spectrum.

We consider here the angular power spectrum of clusters found by an SZ survey. Our aim is to see which parameters (theoretical, cosmological and observational) have the most effect on the cluster angular power spectrum. We calculate the dependence of this power spectrum on several theoretical and cosmological parameters as well as sources of observational noise. This will help identify where the theory needs to be better developed or calibrated by observation or simulation. It may also be a useful guide for observational strategies.

Analytic predictions (based on the extremely good fit of analytic models to dark matter simulations) can predict the expected galaxy cluster counts, masses, and positions. These fits often differ at about the 10% level. In addition, cluster observations generally measure some proxy for the cluster mass (temperature, X-ray flux, SZ flux, velocities, shear in images). These proxies generally depend on more complex astrophysical properties (gasdynamics, for instance, or the state of relaxation of the cluster), and/or are difficult to connect cleanly to the mass (e.g. weak lensing masses, Metzler, White & Loken (2001)). Both the differences in theoretical fits to simulations and the relation of the proxies to the actual mass can modify theoretical predictions; here we quantify their effects for the SZ angular power spectrum.

Several groups have studied SZ properties of clusters in upcoming surveys. Constraints from the angular correlations of clusters found in the SZ have been studied by Moscardini et al (2002), Diaferio et al (2003), Majumdar & Mohr (2003), Mei & Bartlett (2003; 2004), and Wang et al (2004). A similar quantity, the angular correlation of the SZ temperature spectrum, has been considered by Komatsu & Kitayama (1999), Komatsu & Seljak (2002), and Majumdar & Mohr (2003). Battye & Weller (2003) studied similar systematics to those considered here, for number counts as a function of redshift.

In §2, we discuss the selection requirement for the SZ cluster catalogue, §3 defines the angular

---

<sup>6</sup><http://astro.uchicago.edu/spt>

<sup>7</sup><http://astro.estec.esa.nl/SA-general/Projects/Planck>

<sup>8</sup><http://lambda.gsfc.nasa.gov/>

power spectrum and angular correlation function. Our new results are in §4, which considers the theoretical, cosmological and observational uncertainties in the power spectrum and compares them, and §5 concludes. Unless otherwise stated, we will take the hubble constant to be  $h = 0.7$ , baryon fraction  $\Omega_b h^2 = 0.02$ , in a flat  $\Lambda$ CDM universe with  $\Omega_m = 0.3, \Omega_\Lambda = 0.7$ .

## 2. SZ selected galaxy cluster catalogues

An SZ selected galaxy cluster catalogue is one that includes all clusters above a certain minimum SZ flux or (equivalently) above some minimum  $Y$  parameter  $Y_{min}$ . (The  $Y$  parameter is defined in detail below.) For a general review of the SZ effect, see for example Birkinshaw (1999), Rephaeli (1995), and Sunyaev & Zel’dovich (1980). There are two SZ effects, thermal and kinetic. The (frequency dependent) thermal SZ effect is the change in the CMB spectrum due to random thermal motion of the intracluster electrons, and the (frequency independent) kinetic SZ effect is the change in the CMB spectrum due to bulk peculiar motions. The kinetic SZ effect is negligible compared to the thermal SZ effect for the purpose of cluster selection under study here; consequently we restrict our attention to the thermal SZ effect; “SZ effect” hereafter means thermal SZ effect.

The thermal SZ effect can be described in terms of a CMB flux increment or decrement using the  $Y$  parameter, i.e. the integrated  $Y$  distortion

$$\frac{\Delta T}{T_{CMB}} = f(x)Y = f(x) \int d\Omega y(\theta) \quad (1)$$

where the integral is over the SZ emitting regions of the cluster. The prefactor  $f(x) = (x \frac{e^x + 1}{e^x - 1} - 4)(1 + \delta_{rel}(x))$  includes frequency dependence,  $x = h_p \nu / (kT_{CMB}) = \nu / 56.84 GHz$ , and we will neglect the small relativistic correction  $\delta_{rel}$ , which gives only a few percent effect for the hottest clusters (Rephaeli (1995), Itoh et al (1998), Nozawa et al. (2000), Fan & Wu (2003)). The dimensionless Comptonization parameter  $y(\theta)$  is the integration of pressure along the line of sight which passes at an angle  $\theta$  away from the center of the cluster:

$$y(\theta) = \frac{k_B \sigma_T}{m_e c^2} \int d\ell n_e T_e. \quad (2)$$

Here  $\sigma_T, k_B, m_e, n_e, T_e$  are respectively the Thomson cross section, Boltzmann constant, electron mass, intracluster electron density and temperature. The number of electrons along the line of sight to the cluster mass is taken to be

$$d_A^2 \int d\Omega d\ell n_e = \frac{M_{vir} f_{gas}}{\mu_e m_p} \quad (3)$$

where  $d_A = \frac{1}{1+z} \frac{c}{H_0} \int_0^z \frac{1}{E(z')} dz'$ ,  $E(z) = \sqrt{\Omega_m(1+z)^3 + \Omega_\Lambda}$ ,  $M_{vir}$  is the virial mass,  $f_{gas}$  is the intra cluster gas fraction

$$f_{gas} = 0.10 h^{-3/2} M_{15}^{0.148} / (1 + 0.10 M_{15}^{-0.25}) \quad (4)$$

(Lin, Mohr and Stanford (2003)<sup>9</sup>,  $M_{15} = \frac{M_{vir}}{10^{15}h^{-1}M_{\odot}}$ ),  $\mu_e = 1.143$  is the mean mass per electron and  $m_p$  is the proton mass. Then the electron density weighted average temperature

$$\langle T_e \rangle_n = \frac{\int d\ell n_e T_e}{\int d\ell n_e} \quad (5)$$

is given, using virialization arguments (see e.g. Battye & Weller (2003)) by

$$\langle T_e \rangle_n = T_* \left( \frac{M_{vir}}{10^{15}h^{-1}M_{\odot}} \right)^{2/3} (\Delta_c E(z)^2)^{1/3} \left( 1 - 2 \frac{\Omega_{\Lambda}}{\Delta_c} \right) \quad (6)$$

where  $\Delta_c(z) = 18\pi^2 + 82(\Omega_m(z) - 1) - 39(\Omega_m(z) - 1)^2$ . We have taken the  $z$  dependence from Pierpaoli et al (2002). Note this assumes that only electrons within the virial radius are contributing to the SZ effect. Although this form and a specific  $T_*$  can be “derived” using virialization arguments, one can also just define  $T_*$  as the constant of proportionality in the above. The above mass-temperature relation seems to work well for X-ray temperatures of high mass clusters and most measurements of  $T_*$  for the above relation are done in the X-ray. Simulations find  $T_*(\text{X-ray})$  to be  $\sim 1.2$  keV, while observations tend to prefer a higher values,  $T_*(\text{X-ray}) \sim 2.0$  keV (for a recent compilation see, e.g., Huterer & White (2002), and for detailed discussion of subtleties in X-ray temperature definitions see Mathiesen & Evrard (2001) ). There is no a priori reason why the X-ray temperature and the SZ temperature normalizations are identical, as they get the bulk of their signal from different parts of the cluster. In addition, the above is in terms of  $M_{vir}$ , several mass definitions are in use in the literature which can result (White (2001)) in an apparent change in  $T_*$ . Combining these and using again  $M_{15} = \frac{M_{vir}}{10^{15}h^{-1}M_{\odot}}$ , we get

$$\begin{aligned} Y &= \int d\Omega \frac{k_B \sigma_T}{m_e c^2} \int d\ell n_e T_e \\ &= \frac{k_B \sigma_T}{m_e c^2} \frac{f_{gas} M_{vir}}{\mu_e m_p} \frac{1}{d_A^2} T_*^{SZ} M_{15}^{2/3} (\Delta_c E(z)^2)^{1/3} \left( 1 - 2 \frac{\Omega_{\Lambda}}{\Delta_c} \right) \\ &= 1.69 \times 10^3 f_{gas} h \frac{T_*^{SZ}}{\text{keV}} M_{15}^{5/3} (\Delta_c E(z)^2)^{1/3} \left( 1 - 2 \frac{\Omega_{\Lambda}}{\Delta_c} \right) \left( \frac{h^{-1} \text{Mpc}}{d_A} \right)^2 \text{arcmin}^2 \end{aligned} \quad (7)$$

We have used  $T_*^{SZ}$  in the above to emphasize that it is the SZ effect mass temperature normalization which is required for the  $Y$  parameter. The resulting SZ effect is a small distortion of the CMB of order  $\sim 1 mK$ . Results are often quoted in terms of flux, with a conversion

$$F_{\nu} = 2.28 \times 10^4 \frac{x^4 e^x}{(e^x - 1)^2} \left( x \frac{e^x + 1}{e^x - 1} - 4 \right) \frac{Y}{\text{arcmin}^2} mJy \quad (8)$$

For 143 GHz, the  $x$  dependent factor  $\sim -4$  (which translates into  $Y = -\Delta T/T$  for the  $Y$  parameter), for 90 GHz it is -3.3 and for 265 GHz it is +3.4. The SZ effect switches from a decrement to an increment in the CMB spectrum at 218 GHz. Thus, one way of distinguishing the thermal SZ effect from other sources, such as primary anisotropy or noise, is to see if it changes at 218 GHz.

---

<sup>9</sup>Note that for a  $M_{vir} = 10^{14}h^{-1}M_{\odot}$  cluster we get  $f_{gas} = 0.06h^{-3/2}$ . The factor of  $h$  is included to make connection with other definitions, as Lin et al (2003) point out, the variation with  $h$  is not actually a simple scaling. We keep  $h$  fixed in this paper. Note that measurements of  $f_{gas}$  require gas physics theoretical modeling.

Specifics in going from this flux or corresponding  $Y$  value to a cluster detection depend upon the particulars of each experiment. We will consider the idealized case where an SZ experiment will detect all clusters above some minimum  $Y$  value,  $Y_{min}$ . Experiment-specific analysis and followup will be necessary to make reliable cluster identification.<sup>10</sup> Interferometer experiments will “resolve out” some of the power and thus will effectively have a higher  $Y_{min}$ . In addition, false clusters detected due to alignments of low mass SZ sources will need to be discarded via some sort of follow up. The end result of this processing for an SZ cluster survey will be a catalogue of clusters (with angular positions) with SZ decrement above some minimum threshold value  $Y_{min}$ .

We show in figure 2 a plot of the minimum cluster mass for a given  $Y_{min}$  as a function of redshift, for some representative  $Y_{min}$  values expected with APEX and SPT. From above, the minimum mass depends on the mass temperature normalization  $T_*^{SZ}$  which is not well known, we have taken representative values for  $T_*$  from X-ray measurements, which we might expect to be close to  $T_*^{SZ}$ . (Many current SZ measurements take the two to be identical in their analysis.) For  $Y_{min}$  we have taken the APEX’s quoted  $10 \mu\text{K}$  sensitivity and multiplied by a factor of 5, which would be a naive  $5\text{-}\sigma$  detection.  $f_{gas}$  is taken to be  $0.10h^{-3/2}M_{15}^{0.148}/(1 + 0.10M_{15}^{-0.25})$  (Lin, Mohr & Stanford (2003)), in practice it also has a scatter.<sup>11</sup> The slow change in  $M_{min}$  with redshift is a feature of SZ selection, which in principle allows clusters of similar masses to be observed at all distances (Bartlett and Silk (1994), Barbosa et al (1996), Holder et al (2000), Bartlett (2001), Kneissl et al (2001), Diaferio et al (2003)). We can easily calculate observable quantities based on  $M_{min}(Y_{lim}, z)$ . This gives an advantage over X-ray where the flux dims rapidly at higher redshifts. An additional advantage of SZ over X-ray is that the SZ signal strength depends upon the density, while the X-ray signal strength depends upon the density squared. Thus X-ray measurements boost the weight of the cluster core, which has poorly understood physics, in the detection. Conversely, the detection of SZ based on density means that the SZ signal is much more sensitive to line-of-sight contamination (White, Hernquist & Springel (2002)). Specifically, SZ effects are proportional to the total (hot) gas mass in the cluster along the line of sight ( $\Delta T \propto \int n_e T_{gas} dl$ ). In theoretical models the dominant contributions come from the region within  $\sim 0.2 - 0.4$  of the cluster virial

---

<sup>10</sup>One issue is the effect of beam size. For wide beams, confusion from point sources is a significant source of noise, White & Majumdar (2004), Knox et al (2003). For small beams, several pixels must be combined to produce the total cluster signal (see for example Battye & Weller (2003)) above the  $Y_{min}$  threshold, and there may be errors inherent to the corresponding cluster finding. These can be dealt with both in the data acquisition (e.g. by having more frequencies and an appropriate scanning strategy to help identify the point sources) and in the analysis; the effects particular to an experiment will depend strongly on the details of that experiment. An early example finding clusters in a noisy map was done by Schulz & White (2003), a more recent start-to-finish analysis of N-body simulations, including cluster finding and noise modeling, has been done for Planck SZ clusters by Geisbusch, Kneissl & Hobson (2004).

<sup>11</sup>The scatter found by Lin et al (2003) gives

$$f_{gas} = 0.10(\pm 3\%)h^{-3/2}M_{15}^{0.148 \pm 27\%}/(1 + 0.10(\pm 6\%)M_{15}^{-0.25 \pm 28\%}) . \quad (9)$$

Mass cut

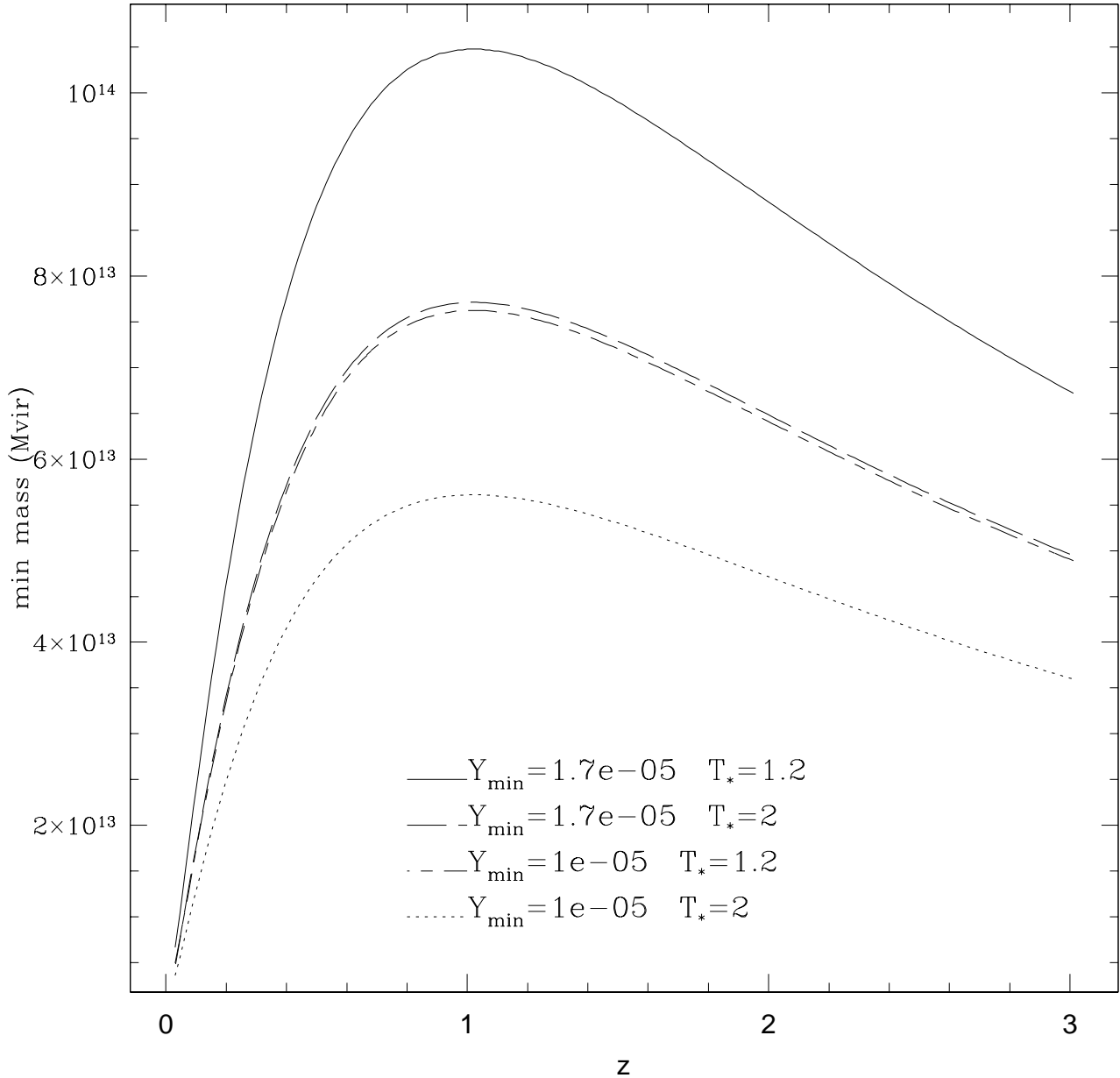


Fig. 1.— Minimum mass for given  $Y_{\min}$  using equation 7. Note that as  $Y_{\min} \propto T_*^{SZ} (M_{\min})^{5/3}$ , fixed  $Y_{\min}/T_*^{SZ}$  will give the same  $M_{\min}$ . At 143 GHz,  $Y = -\Delta T/T$ , at 150 GHz, corresponding to APEX,  $Y = -0.96\Delta T/T$ . Note that these are virial masses  $M_{\text{vir}}$ ,  $M_{200}$  will be smaller by a factor of 0.77, see section §4.

radius (Komatsu & Seljak (2002)). Note that at low redshifts the SZ selection probes very low mass objects, where the poorly understood gas physics dominates; as a result we will take a minimum redshift cut of  $z = 0.2$ . Such a cut could be imposed experimentally in the followup.

### 3. Analytic calculations

In order to go from this cluster catalogue to cosmologically useful mass counts, theoretical processing and assumptions are needed. In this section we review and set the notation for the angular power spectrum/correlation function in terms of analytic quantities (which will be varied in the next section). Theoretical inputs to the analytic calculations include the choice of mass function, transfer function, biasing scheme, mass temperature relations (in particular  $T_*^{SZ}$ ), the initial power spectrum and of course cosmological parameters. Some of these, such as the mass function, are well tested, other quantities such as  $T_*^{SZ}$ , the mass temperature normalization appropriate for calculating the  $Y$  parameter, are not determined well at all either theoretically or observationally, and widely varying approximations are in use. We will compare these approximations in the following. The angular power spectrum/correlation function can be calculated with analytic prescriptions for the mass function  $dn/dM(z)$  and the bias relating the dark matter correlations to the correlations for the galaxy clusters. The two dimensional correlation function is (Moscardini et al (2002), Diaferio et al (2003), Mei & Bartlett (2003)):

$$w(\theta) = \frac{\int_0^\infty r_1^2 dr_1 \int_0^\infty r_2^2 dr_2 \int_{M_{min}(Y_{min})}^\infty dM_1 \int_{M_{min}(Y_{min})}^\infty dM_2 \phi(M_1, r_1) \phi(M_2, r_2) \xi(M_1, M_2, \mathbf{r}_1 - \mathbf{r}_2)}{[\int_0^\infty r^2 \int_{M_{min}(Y_{min})}^\infty dM \phi(M, r) dr]^2} \quad (10)$$

where  $r_1, r_2$  are the radial distances of the clusters which have three dimensional positions  $\mathbf{r}_1, \mathbf{r}_2$  and  $\mathbf{r}_1 \cdot \mathbf{r}_2 = r_1 r_2 \cos \theta$ .  $\xi(M_1, M_2, \mathbf{r}_1 - \mathbf{r}_2)$  is the three dimensional cluster correlation function and  $\phi(M, r)$  is the selection function (as a function of radial distance). In particular,

$$\phi(M, r) = \frac{dn}{dM}(z(r)) \quad (11)$$

$$\xi(M_1, M_2, \mathbf{r}_1 - \mathbf{r}_2) = b(M_1, z_1(r_1)) b(M_2, z_2(r_2)) \xi_{dm}(\mathbf{r}_1 - \mathbf{r}_2) \quad (12)$$

$$\xi_{dm}(\mathbf{r}_1 - \mathbf{r}_2) = \xi_{dm}(r) = \int \Delta^2(k) \frac{\sin kr}{kr} d \ln k, \quad r = |\mathbf{r}_1 - \mathbf{r}_2| \quad (13)$$

$$\Delta^2(k) = \frac{V}{(2\pi)^3} 4\pi k^3 P(k) \quad (14)$$

$$P_{lin}(k) = D^2(z) P_0 k^n T^2(k) \quad (15)$$

In the above, the selection function is the number of clusters as a function of redshift (with the normalization included explicitly). The linear power spectrum  $P_{lin}$  comes from an initial power spectrum with slope  $n$ , normalization  $P_0$  implied by our choice of  $\sigma_8$ , and transfer function  $T^2(k)$ . The nonlinear power spectrum is derived from  $P_{lin}$  using the method of Smith et al (2002). The linear bias  $b$  is also defined above, nonlinear bias will be considered in the next section.

The full two-dimensional correlation function thus becomes

$$\begin{aligned}
 w(\theta) &= \frac{\int_0^\infty r_1^2 dr_1 \int_0^\infty r_2^2 dr_2 \int_{M_{\min}(Y_{\min})}^\infty dM_1 \frac{dn}{dM_1}(z(r_1)) \int_{M_{\min}(Y_{\min})}^\infty dM_2 \frac{dn}{dM_2}(z(r_2)) b(M_1, z_1(r_1)) b(M_2, z_2(r_2)) \xi_{dm}(|r_1 - r_2|)}{[\int_0^\infty r^2 \int_{M_{\min}(Y_{\min})}^\infty dM \frac{dn}{dM}(z(r)) dr]^2} \\
 &= \int_0^\infty r_1^2 \Phi(r_1) \int_0^\infty r_2^2 dr_2 \Phi(r_2) \xi_{dm}(|r_1 - r_2|)
 \end{aligned} \tag{16}$$

where we have defined a generalized selection function (Moscardini et al (2002), Mei & Bartlett (2003)<sup>12</sup>)

$$\Phi(r) = \frac{\int_{M_{\min}(Y_{\min})}^\infty dM \frac{dn}{dM}(z(r)) b(M, z(r))}{[\int_0^\infty r^2 \int_{M_{\min}(Y_{\min})}^\infty dM \frac{dn}{dM}(z(r)) dr]} \tag{17}$$

The above angular correlation function (and corresponding power spectrum) can be simplified via the Limber approximation (1953). As  $\Phi$  varies slowly relative to the correlation function, the integration can be rewritten as an integration over an average distance  $y \equiv (r_1 + r_2)/2$  and one over relative separations  $x = (r_1 - r_2)$ . The integration over  $x$  then gives a Bessel function  $J_0$ :

$$\begin{aligned}
 w(\theta) &\sim \int dy y^4 \Phi(y)^2 \int dx \xi_{dm}(\sqrt{y^2 \theta^2 + x^2}) \\
 &= \int dy y^4 \Phi(y)^2 \int d \ln k \pi J_0(ky\theta) \frac{\Delta^2(k)}{k}
 \end{aligned} \tag{18}$$

Then the power spectrum

$$C_\ell = 2\pi^2 \int dy y^5 \Phi(y)^2 \frac{\Delta^2(\ell/y)}{\ell^3} \tag{19}$$

can be read off in the small angle approximation

$$\begin{aligned}
 w(\theta) &= \frac{1}{4\pi} \sum_\ell \sum_{m=-\ell}^{m=+\ell} |a_\ell^m|^2 P_\ell(\cos\theta) \\
 &= \sum_\ell \frac{2\ell+1}{4\pi} C_\ell P_\ell(\cos\theta) \\
 &\simeq \int d\ell \frac{\ell}{2\pi} C_\ell J_0(\ell\theta)
 \end{aligned} \tag{20}$$

because  $P_\ell(\cos\theta) \simeq J_0(\ell\theta)$  for small angle. We can also define the inverse via

$$C_\ell = 2\pi \int_0^\infty w(\theta) J_0(\ell\theta) \theta d\theta \tag{21}$$

The correlation function  $w(\theta)$  and its power spectrum  $C_\ell$  can be transformed to each other by the above equation, and therefore they encode the same information. However, to understand possible measurements and errors, use of  $C_\ell$  is usually preferable because the errors for different  $\ell$  values are uncorrelated for small  $\ell$ . We'll use  $C_\ell$  for the most part in the following.

For reference, we show in figure 3 the angular correlation function for a representative model. The dependence on the possible reasonable choices for the analytic and cosmological model parameters is the subject of a later section. The choices taken here will be our “vanilla” model: for the

---

<sup>12</sup>Note our selection function differs from that in Mei & Bartlett (2003) by the factor  $r^2 dr/dz$ , their expression for  $w(\theta)$  is equivalent.

“Vanilla” model

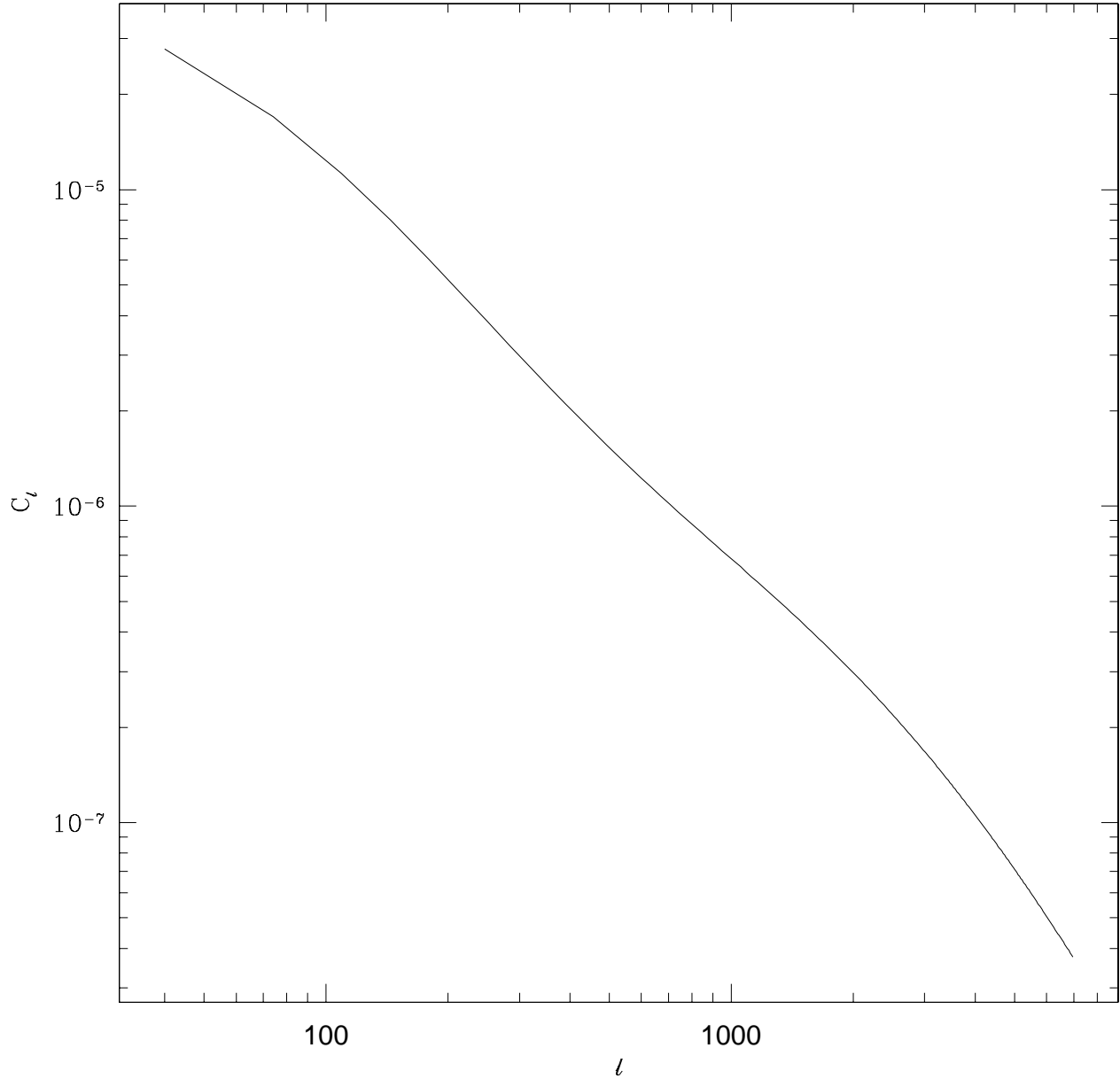


Fig. 2.— Our reference “vanilla” model. The Evrard mass function, Sheth-Tormen bias, Eisenstein-Hu transfer function,  $T_*^{SZ} = 1.2$ ,  $f_{gas} = 0.10h^{-3/2}M_{15}^{0.148}/(1 + 0.10M_{15}^{-0.25})$ ,  $\sigma_8 = 0.9$ ,  $n = 1$ ,  $\Omega_m = 0.3$ ,  $\Omega_b h^2 = 0.02$  and for experimental parameters  $Y_{min} = 1.7 \times 10^{-5}$  and minimum redshift  $z_{min} = 0.2$ . Mass conversions have been taken into account with the prescription given in White (2001).

dark matter we use the Evrard mass function, the Sheth-Tormen bias and the Eisenstein-Hu transfer function, for cluster parameters we take  $T_*^{SZ} = 1.2$ ,  $f_{gas} = 0.10h^{-3/2}M_{15}^{0.148}/(1 + 0.10M_{15}^{-0.25})$ , for cosmological parameters we take  $\sigma_8 = 0.9$ ,  $n = 1$ ,  $\Omega_m = 0.3$ ,  $\Omega_b h^2 = 0.02$  and for experimental parameters we take  $Y_{min} = 1.7 \times 10^{-5}$ . Our minimum redshift is  $z_{min} = 0.2$ . We will use the same axes for (almost) all the plots, so that the relative impact of different effects are easily comparable. For these parameters, one gets about 10 clusters per square degree.

The basic expression above has been used by Mei and Bartlett (2003) and a variant (to be discussed later) has been derived and used by Diaferio et al (2003). We have extended these authors’ work in this review section by implementing the mass conversions and including scatter due to the cluster parameter uncertainties. We also differ Mei and Bartlett in using the Eisenstein-Hu transfer function. Our calculation of the  $C_\ell$  from SZ selected galaxy clusters is also new, as stated above, we prefer it for its better control of errors.

#### 4. Uncertainties

We now compare the effects of modeling, cosmological and observational uncertainties/unknowns on the cluster angular power spectrum. Some aspects of these, with different assumptions, have been considered previously for the cluster angular correlation function: Diaferio et al (2003) consider two cosmological models and vary  $Y_{min}$  and the bias, Mei and Bartlett (2003; 2004) vary  $Y_{min}$ ,  $\sigma_8$ ,  $\Omega_m$  and  $T_*^{SZ}$ . For the angular power spectrum in a Fisher matrix analysis, Wang et al (2004) vary these and the primordial fluctuation spectrum, the dark energy density and equation of state, the baryon density, and also in the  $Y(M)$  relation allow extra  $(1 + z)$  and  $M$  factors to appear. Majumdar & Mohr (2002; 2003) vary most of these factors as well in finding their constraints. Except for the Mei & Bartlett (2004) paper which considers APEX, these other experiments are primarily concerned with far future experiments such as SPT.

One of the new aspects of this work is comparing these recognized uncertainties with other theoretical uncertainties (nonlinear bias, different mass functions) and with errors for APEX-SZ, an experiment which is not far-future. In addition, as mentioned earlier, we are primarily concerned with the angular power spectrum as in the last two works, rather than the correlation function so that the errors can be more easily compared to these uncertainties.

**Cosmological model dependence** We start by showing what changes to the cosmological model do to the “vanilla” model, for later comparison with the modeling and experimental uncertainties. For instance, the current published joint WMAP/SDSS cosmological parameters and errors are  $\Omega_m = 0.30 \pm 0.04$ ,  $\sigma_8 = 0.86_{-0.11}^{+0.18}$  (Tegmark et al (2004)). We compare our “vanilla” model with changes in  $\Omega_m$ ,  $\sigma_8$ , respectively in figure 4 to show cosmological parameter differences compete with the  $Y(M)$  modeling differences. The correlation function decreases with increasing  $\sigma_8$ , as a higher  $\sigma_8$  means more clusters everywhere and especially at large distances, and thus more non-correlated clusters nearby any given cluster. By explicitly fitting, we found that the scaling of

Cosmological parameter dependence

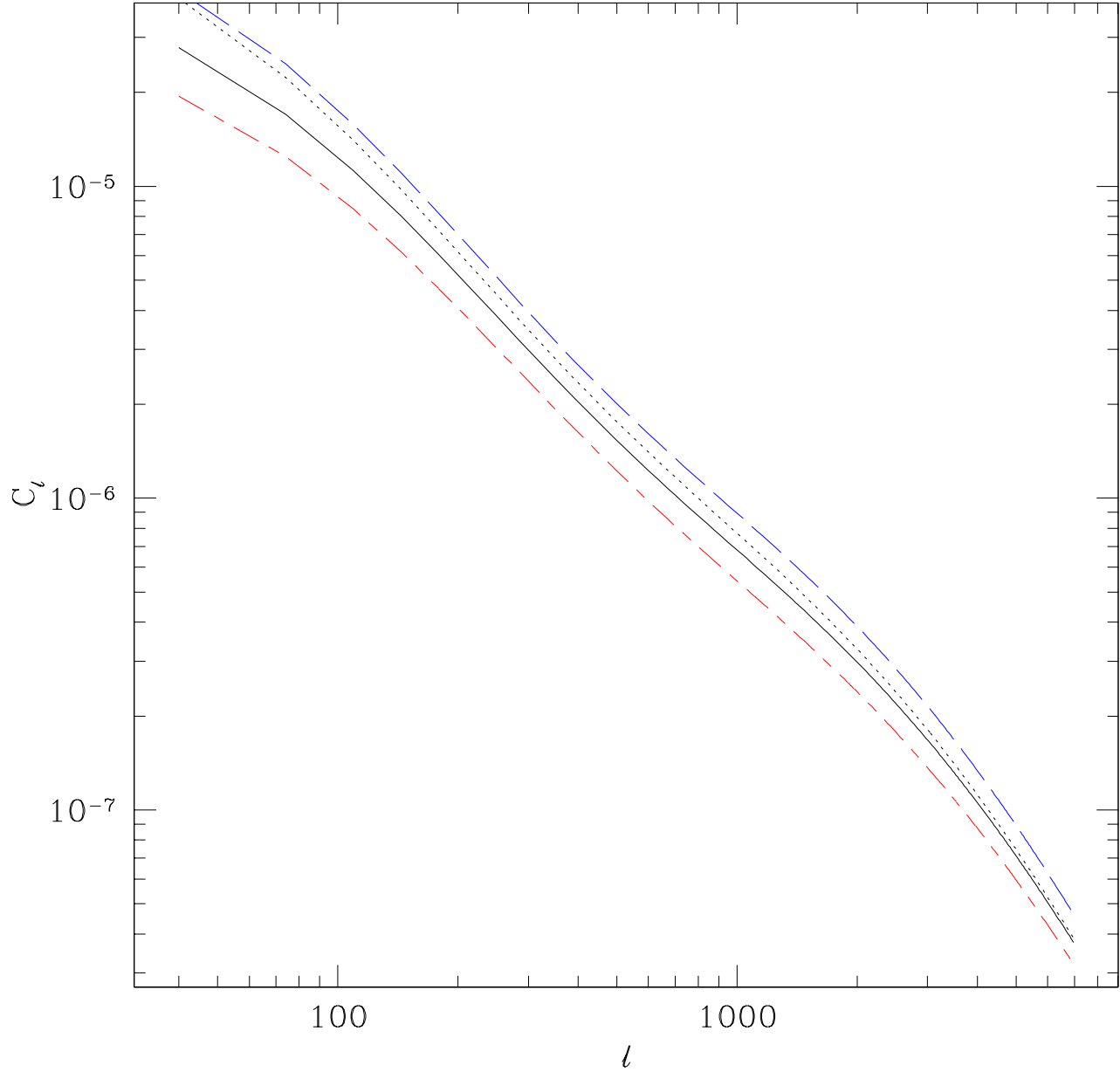


Fig. 3.— The dependence of the power spectrum on varying  $\sigma_8$  and  $\Omega_m$  separately. The solid line is our reference vanilla model with  $\sigma_8 = 0.9, \Omega_m = 0.3$ . The long dashed line is for  $\sigma_8 = 0.8$ , the short-long dashed line is for  $\sigma_8 = 1.0$  and the dotted line is for  $\Omega_m = 0.25$ .

the  $C_\ell$  with linear bias goes roughly as  $\sigma_8^{-1.4-\alpha(\ell)}$  where  $\alpha(\ell)$  ranges from around zero for  $\ell \sim 100$  to about 0.9 for  $\ell \sim 6000$ .

In fact, the effect of changing  $\sigma_8$  is somewhat smaller, as there are other constraints which must be satisfied when changing  $\sigma_8$ , for instance the observed and hence fixed number counts of clusters. One can include this constraint by requiring the number of clusters to remain fixed along with  $\Omega_m$  for instance, and find the required scaling between  $T_*^{SZ}$  and  $\sigma_8$  (Sadeh & Rephaeli (2004)). Allowing  $\Omega_m$  to vary still gives a constraint using identical arguments to Huterer & White (2002) (also see Evrard et al (2002)) who were considering the X-ray temperature: Fixing the number of clusters with a given  $Y$  parameter (an observable) and allowing  $T_*^{SZ}$ ,  $\sigma_8$  and  $\Omega_m$  to vary gives the following (directly analogous to X-ray) scaling relation,

$$T_*^{SZ} \sim (\sigma_8 \Omega_m^{0.6})^{-1.1} . \quad (22)$$

More precisely it will be  $f_{gas} T_*^{SZ}$  on the left. The modeling parameter  $T_*^{SZ}$  will be discussed in detail in the next section.

#### 4.1. Modeling Uncertainties

There are several parameters and functions that go into the theoretical predictions: cluster properties independent of the SZ effect, the transformation from cluster mass to the observable  $Y$  (equation 7), and the background cosmology parameters. For an SZ selected survey, uncertainties in modeling affect results by bringing objects into or out of the survey. As a result, uncertainties that have a large effect on the observational properties of the lowest mass clusters in the survey ( $M_{vir} \sim 10^{14} h^{-1} M_\odot$ ) have the most impact.

**Dark matter cluster properties:** The cluster properties independent of the SZ effect used in the analytic prediction of  $C_l$ , equation(19), are the correlation function of the dark matter, the mass function, and the bias. The dark matter correlation function is quite well known, and can be obtained from the initial power spectrum via a transfer function (such as BBKS (1986) or Eisenstein & Hu (1997)) and then by implementing a nonlinear power spectrum prescription (such as Peacock and Dodds (1996) or Smith et al (2002)).

Before defining the mass functions, it should be recalled that there are several different mass definitions in use. For SZ calculations, the mass-temperature relation usually involves the virial mass, but the popular mass functions usually are instead for some linking length or parameter  $\Delta$  such that the mass inside a radius  $r_\Delta$  is  $\Delta$  times the critical density<sup>13</sup>:

$$M_\Delta = \frac{4\pi}{3} \Delta \rho_{crit} r_\Delta^3 = \int_0^{r_\Delta} 4\pi r^2 dr \rho(r) . \quad (23)$$

---

<sup>13</sup>Note that some people use  $\Delta$  to refer to the density relative to the mean density.

This mass can differ significantly from the virial mass (White (2001)), which enters into the definition of  $Y$ , and conversion must be made between the virial mass and the mass appearing in the mass function. The way suggested in White (2001) is to assume an NFW (Navarro, Frenk and White (1997)) mass profile to do this, a fitting formula for this method is given in Hu & Kravtsov (2003). For instance, in an  $\Omega_m = 0.3$  universe,  $M_{vir}/M_{200} \sim 1.3$  for a cluster with concentration 5.

There are three commonly used mass functions which can be viewed as generalizations of the heuristic mass function of Press and Schechter (1974). These are based upon simulations with large enough volume to accurately sample the number of rare objects such as galaxy clusters: the Jenkins et al (2001) mass function, the Sheth-Tormen (1999) mass function and the Evrard et al (2002) mass function. The first two are the masses in terms of  $M_{180\Omega_m}$ , while the last is in terms of  $M_{200}$ . These mass functions are expressed in terms of  $\sigma(M, z)$  or  $\nu(M, z)$ . Here  $\sigma(M, z)$  is the rms of the mass density field smoothed on a scale  $R = (3M/(4\pi\rho_b))^{1/3}$  with a top hat window function,  $\sigma(M, z) = \int_0^\infty \frac{dk}{k} \Delta^2(k) \tilde{W}_M^2(k, z)$  where  $\tilde{W}_M^2(k, z)$  is the Fourier transform of window function,  $\nu = \delta_c/\sigma$ , and  $\rho_b = \Omega_m \rho_{crit}$ . We ignore the weak cosmological dependence of  $\delta_c$  and set  $\delta_c \equiv 1.686$ . We then can write

$$\frac{dn}{dM} = \frac{\rho_m(z)}{M} f(\ln \sigma^{-1}) \frac{d \ln \sigma^{-1}}{dM}; \quad (24)$$

to get

mass function	$\Delta\rho_{crit}$	$f(\ln \sigma^{-1})$	
Sheth – Tormen	$180\rho_b$	$\frac{0.364}{\sigma}(1 + 0.811\sigma^{0.6})e^{-\frac{1}{\sigma^2}}$	(25)
Jenkins	$180\rho_b$	$0.301 \exp[- \ln \sigma^{-1} + 0.64 ^{3.82}]$	
Evrard et al	$200\rho_{crit}$	$0.22 \exp[- \ln \sigma^{-1} + 0.73 ^{3.86}]$	

The mass density field and the correlation function are derived from the primordial power spectrum, which we take to be scale free, i.e.  $n = 1$ , and normalized by  $\sigma_8$ . We use the Eisenstein & Hu (1997) transfer function which is within 3% of the exact CMB power spectrum (M. White, private communication), and obtain the corresponding nonlinear dark matter power spectrum with the fit by the Smith et al (2002). The earlier transfer functions are less accurate. These are all fairly recent and different mass and transfer functions produce different  $C_\ell$  accordingly. For instance, the (less accurate) earlier BBKS (1986) transfer function decreases  $C_\ell$  by 9% at  $\ell = 214$ , the Sheth-Tormen mass function (1999) decreases it by 19%, while using the Peacock & Dodds (1996) nonlinear prescription gives no noticeable change. A comparison of Sheth-Tormen, Evrard and Jenkins mass functions and the corresponding  $C_\ell$  are given in figure 4.

There are also several different possibilities for bias. The (linear) bias  $b(M, z)$  is defined via

$$\xi(M, M, r, z) = b^2(M, z)\xi(r, z) \quad (26)$$

where  $\xi(r, z)$  is the dark matter power spectrum and  $\xi(M, M, r, z)$  is the power spectrum of halos of mass  $M$ . The original idea of peak biasing by Kaiser (1984) has been improved upon with fits to simulations. There is the Sheth-Tormen bias (1999), fit to simulations and motivated by a moving wall argument, the bias found by Sheth, Mo & Tormen (2001), and the bias more recently found

Mass function dependence

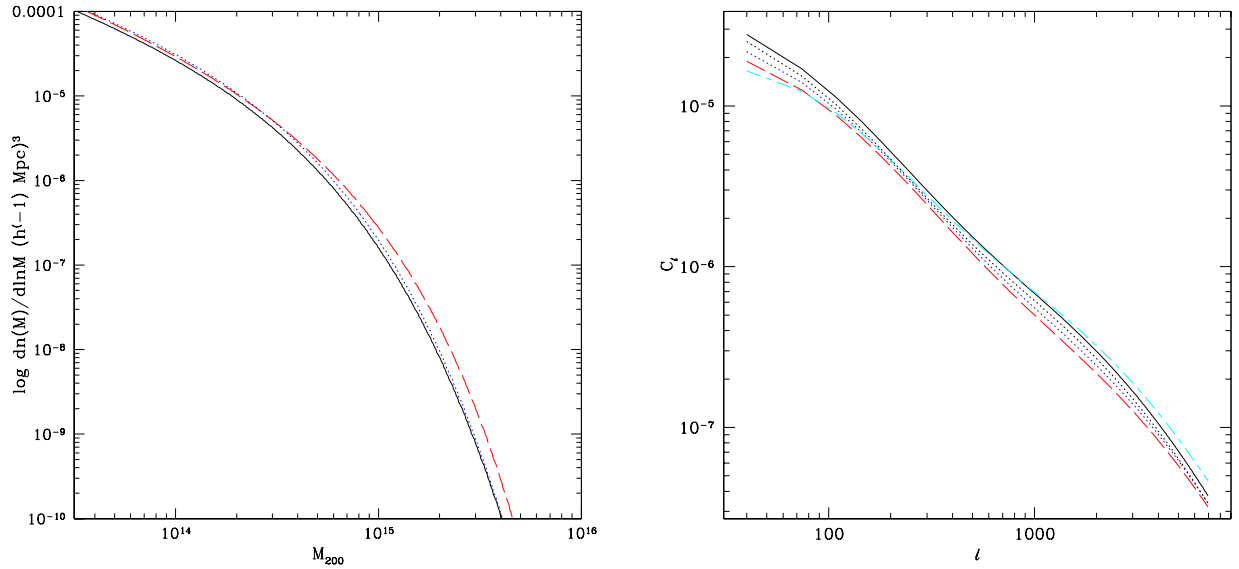


Fig. 4.— On left: Evrard et al, Jenkins et al and Sheth-Tormen mass functions. The smooth line is the Evrard mass function, the dotted line is the Jenkins mass function and the dashed line is the Sheth-Tormen mass function. On right: the corresponding angular power spectra, plus the vanilla model except for BBKS transfer function (dot-dashed line) and vanilla model without using mass function conversion for mass-temperature (heavy dotted line).

by Seljak and Warren (2004). The Seljak and Warren bias was found for small masses but has the best statistics currently available. It overlaps closely with the Sheth-Tormen bias where it is valid but is systematically lower and does not extend very far into the high mass range needed for clusters. Thus, using a combination of the two biases would result in a bias which doesn't integrate to one when combined with the Sheth-Tormen mass function. Consequently we have taken the Sheth-Tormen bias as our default.

bias function	$\Delta\rho_{crit}$	bias	
Sheth – Tormen	$180\rho_b$	$1 + \frac{1}{\delta_c}(\nu'^2 - 1) + \frac{2p}{\delta_c(1+\nu'^{2p})}$	$\nu' = \sqrt{0.707}\delta_c/\sigma = 1.418/\sigma, p = 0.3$
Sheth, Mo, Tormen	$180\rho_b$	$1 + \frac{1}{\delta_c} \left[ \nu'^2 + b\nu'^{2(1-c)} - \frac{\nu'^{2c}/\sqrt{a}}{\nu'^{2c} + b(1-c)(1-c/2)} \right]$	(27)
$a = 0.707, b = 0.5, c = 0.6$			
Seljak&Warren	$200\rho_{crit}$	$0.53 + 0.39x^{0.42} + \frac{0.08}{40x+1} + 10^{-4}x^{1.7}$	$x = M/M_{nl} \quad M = M_{nl} \leftrightarrow \nu = \sigma$

For the SZ selected power spectrum one integrates over all masses greater than some  $M_{min}(Y_{min}, z)$ , so that what one is actually probing is an integral of the bias, i.e.  $\Phi(Y_{min}, z)$  in equation 17. One can define a related (rescaled by the number density) quantity:

$$b_{method,eff} = \frac{\int_{M_{min}(Y_{min})}^{\infty} dM \frac{dn}{dM}(z(r)) b_{method}(M, z(r))}{\frac{dn}{dm}(z(r))} \quad (28)$$

where  $b_{method}$  is one of the above biases. The linear biasing prescription above doesn't work as well for short distances, and for this a ‘‘scale dependent bias’’ has been calculated for the cluster correlation functions by Hamana et al (2001) and Diaferio et al (2003). This scale dependent bias is also a function of the separation  $r$  of the objects of interest and for Diaferio et al is

$$b_{eff}(r, z, Y_{min}) = b_{ST,eff}(z, Y_{min})(1 + b_{ST,eff}(z, Y_{min})\sigma(r, z))^{0.35} \quad (29)$$

the corresponding expression for Hamana et al has an exponent 0.15. Diaferio et al have shown that this bias works well for cluster correlation functions for a range of redshifts. We will use the Diaferio et al case for illustration. The bias of Hamana et al is midway between the linear biasing case and the Diaferio et al case (2003). With this bias, the correlation function becomes

$$w(\theta) = \int_0^{\infty} r_1^2 \Phi(r_1) \int_0^{\infty} r_2^2 dr_2 \Phi(r_2) \tilde{\xi}_{dm}(|r_1 - r_2|) \quad (30)$$

where

$$\tilde{\xi}_{dm}(|r_1 - r_2|) = (1 + b_{ST,eff}(z, Y_{min})\sigma(r, z))^{0.70} \xi_{dm}(|r_1 - r_2|) \quad (31)$$

In the Limber approximation one then finds

$$w(\theta) = \int dy y^4 \Phi(y)^2 \int dx (1 + b_{ST,eff}(z, Y_{min})\sigma(\sqrt{y^2\theta^2 + x^2}, z))^{0.70} \xi_{dm}(\sqrt{y^2\theta^2 + x^2}) \quad (32)$$

As this doesn't easily allow a rewriting in terms of  $J_0(\ell\theta)$ , obtaining the power spectrum  $C_\ell$ 's is somewhat more difficult. In figure 4.1 we show the correlation function  $w(\theta)$  at left and the power spectrum  $C_\ell$  at right for the vanilla model and then the Sheth, Mo & Tormen linear bias and the Diaferio et al nonlinear bias. We transformed the difference of  $w(\theta)$ 's between the vanilla model and Diaferio et al model to get the  $C_\ell$ 's for the former. We use the vanilla model parameters for the Diaferio et al bias (e.g.  $T_*^{SZ} = 1.2$  rather than  $T_*^{SZ} = 2.0$  as they did). There is also intrinsic scatter around the bias and the mass functions. We will not put this in explicitly, however the weak dependence on the scatter in the  $Y(M)$  relation (mentioned below) leads us to suspect it will not be a large effect.

**Y parameter:** The next step is relating the cluster mass to a  $Y$  parameter, which involves more complicated gas physics. In addition, the increased sensitivities of upcoming experiments will allow smaller and smaller mass clusters to be detected, which are more and more easily disrupted by this gas physics. Moscardini et al (2002) and Mei & Bartlett (2003) have considered some effects of ICM properties on the correlation function.

There are actually three questions: the actual form of the mass temperature/ $Y$  parameter relation, the normalization of this relation (i.e.  $T_*^{SZ} f_{gas}$ ) and the scatter around this normalization for a representative group of galaxy clusters. Simulations alone cannot determine these: the heating and cooling properties of clusters are not understood at an accuracy needed for precision cosmology and so these questions are intermingled by assumptions used. For instance, the scaling relation was obtained by assuming an isothermal gas profile. Assuming hydrostatic equilibrium and using the total  $Y$  parameter means that the details of the profile (many others have been suggested, e.g. Komatsu & Seljak (2001), Loken et al (2002)) get absorbed into the mass temperature (or  $Y$  parameter) normalization or form. If the parameters of the gas profile change with cosmology, it's possible that the normalization will also do so, or rather the form of the  $Y(M)$  relation, a possibility which will need to be checked for carefully in the data. We consider the form of the mass temperature/ $Y$  parameter relation, the normalization, and the scatter in turn.

There are several different mass temperature relations in the literature (see Sadeh & Rephaeli (2004) for a description of five common ones), usually based on X-ray mass temperature relations. These relations have been tested both with observations and simulations (bear in mind again that the simulations do not seem to yet have all the necessary physics), and some generalizations of these relations have also been tested. For instance, equation 7 can be generalized to include different  $z$  and  $M$  dependence, such as multiplying by a factor  $(1+z)^\gamma M^\alpha$ . The mass- $Y$  parameter relation also has dependence on  $f_{gas}$  which can be generalized to change  $f_{gas}$  with redshift, or change it differently with mass. Observational data and simulation data have been used to search for these effects.

Most observational tests are of the X-ray mass temperature relations and of the change of  $f_{gas}$  with mass or redshift, rather than of the  $Y(M)$  relation. For example, Ettori et al (2004a) have found no evidence for additional evolution in redshift of the mass temperature relation. For scaling of mass with temperature, Ettori et al (2004b) and Ota & Mitsuda (2004) find  $T_{gas}^{X-ray} \sim M^{2/3} - M^{3/5}$ ,

Bias dependence

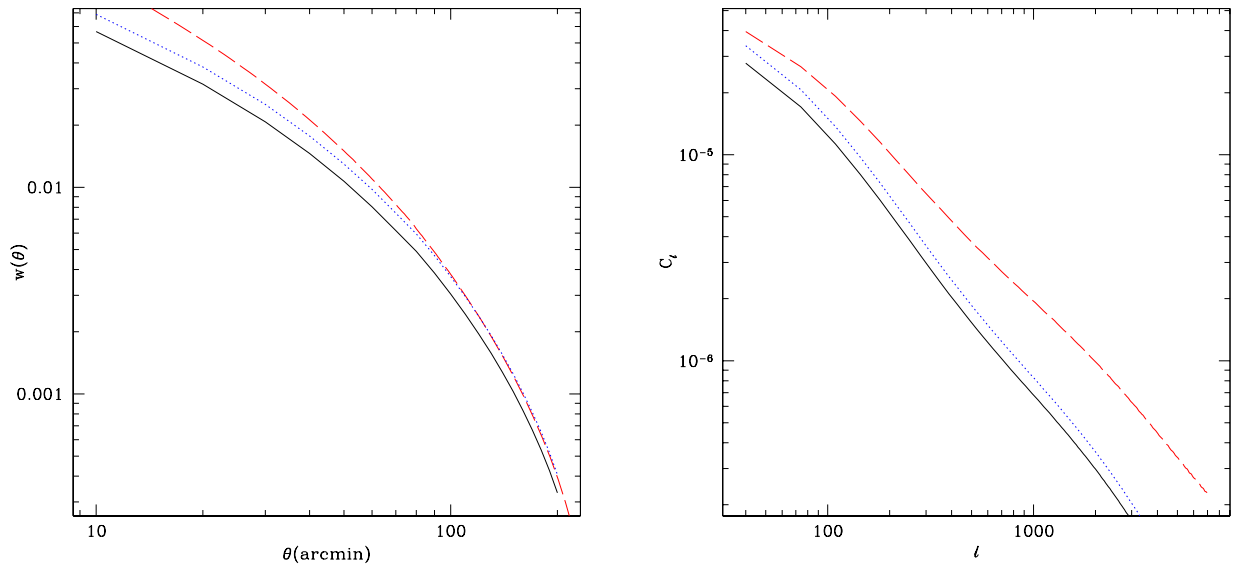


Fig. 5.— The effect of different bias prescriptions on the correlation function  $w(\theta)$  (left) and the power spectrum  $C_\ell$  (right). The vanilla reference model is shown in both cases (solid line), as well as the cases with the Sheth Mo & Tormen bias in equation 27 (dotted line) and the nonlinear bias of Diaferio et al, equation 29 (dashed line).

but the departure from the  $M^{2/3}$  relation is about  $1.5\sigma$  for the Ettori et al data and is marginal given the error bars for the Ota & Mitsuda data. The former group also finds marginal (less than  $2\sigma$ ) evidence for clusters of a fixed temperature to have smaller gas mass at high redshift. We have already included the  $f_{gas}$  dependence with mass found by Lin et al (2003), but have not included any redshift dependence.

More simulations than observations have addressed the  $z$  and  $M$  dependences of the  $Y(M)$  relation directly. For example daSilva et al (2004) find numerically that the  $z$  dependence seems to be well represented by the simple scaling given in equation 7. For lower mass objects da Silva et al (2004) find that the  $M$  dependence in the  $Y(M)$  relation steepens from  $M^{5/3}$ . Our use of an  $M$ -dependent  $f_{gas}$  produces an effect in the same direction. However, for clusters with  $M_{200}$  above  $5 \times 10^{13} h^{-1} M_{\odot}$  (or  $M_{vir} > 6.5 \times 10^{13} h^{-1} M_{\odot}$ ), one finds that this can just be absorbed into scatter of about 10 % around the  $M^{5/3}$  scaling (White et al (2002)) in the  $Y(M)$  relation. Detailed studies of effects of changes of the mass-Y parameter relation with redshift on cosmological parameter estimation have been done by Majumdar & Mohr (2003).

For normalization, we have combined all the mass temperature conversion ignorance into the parameter combination  $Y \propto T_*^{SZ} f_{gas}$ . The simplest procedure would be to say that  $Y = Y_{vir}$  (and that gas outside this radius does not contribute significantly) and to take  $T_*^{SZ}$  to be the X-ray value,

$$T_*^{SZ} \equiv T_*^{X-ray} . \quad (33)$$

As noted in section §2, there is strong disagreement between simulations and observations for  $T_*^{X-ray}$ . Thus the parameter  $T_*^{X-ray}$  is not well determined. Even if it were, using it to normalize the  $Y(M)$  relation is not necessarily justified. For the SZ effect, the normalization has an additional contribution due to line of sight contamination from gas outside the cluster. If one takes simulation results (which should be taken with a grain of salt given the above mentioned discrepancy), this projection effect on  $Y(M)$  raises the normalization about 8% (White et al (2002)) above the normalization due to the cluster alone. The differences between power spectra for different normalizations of the  $Y(M)$  relation are shown in figure 4.1. We also show that taking  $f_{gas}$  fixed at  $0.06 h^{-1}$  (the value for a cluster with  $M_{vir} = 10^{14} h^{-1} M_{\odot}$ ) gives a power spectrum very close to the vanilla model. And we additionally have shown a model with  $T_*^{SZ} = 2.2\text{keV}$  which has the 8% increase from line of sight projection (from  $T_*^{SZ} = 2\text{keV}$ ). Of course, as changing  $T_*^{SZ} f_{gas}$  just rescales the  $Y$  parameter, raising  $T_*^{SZ} f_{gas}$  is equivalent to lowering  $Y_{min}$ , i.e. one is probing clusters with smaller mass.

The intrinsic scatter in the mass temperature relation (about 10 -12% from Evrard, Metzler & Navarro (1996) for X-ray simulations and similarly from White et al (2002) for SZ simulations) had less than a percent effect on the  $C_{\ell}$ , even with APEX sensitivity and accompanying very low mass cuts. For a large scatter of about 30%,  $C_{\ell}$  was roughly decreased by about 3%. A similar robustness to M-T scatter was found in the Fisher matrix calculations (Levine, Schulz & White (2002)) and in that of number counts (Battye & Weller (2003)). Metzler (1998) also found from simulations that the scatter in the mass temperature relation was larger than that for the mass-Y parameter relation. Thus for the bulk of the paper, we have used equation 7 and combined all our ignorance

Y(M) and mass-temperature normalization dependence

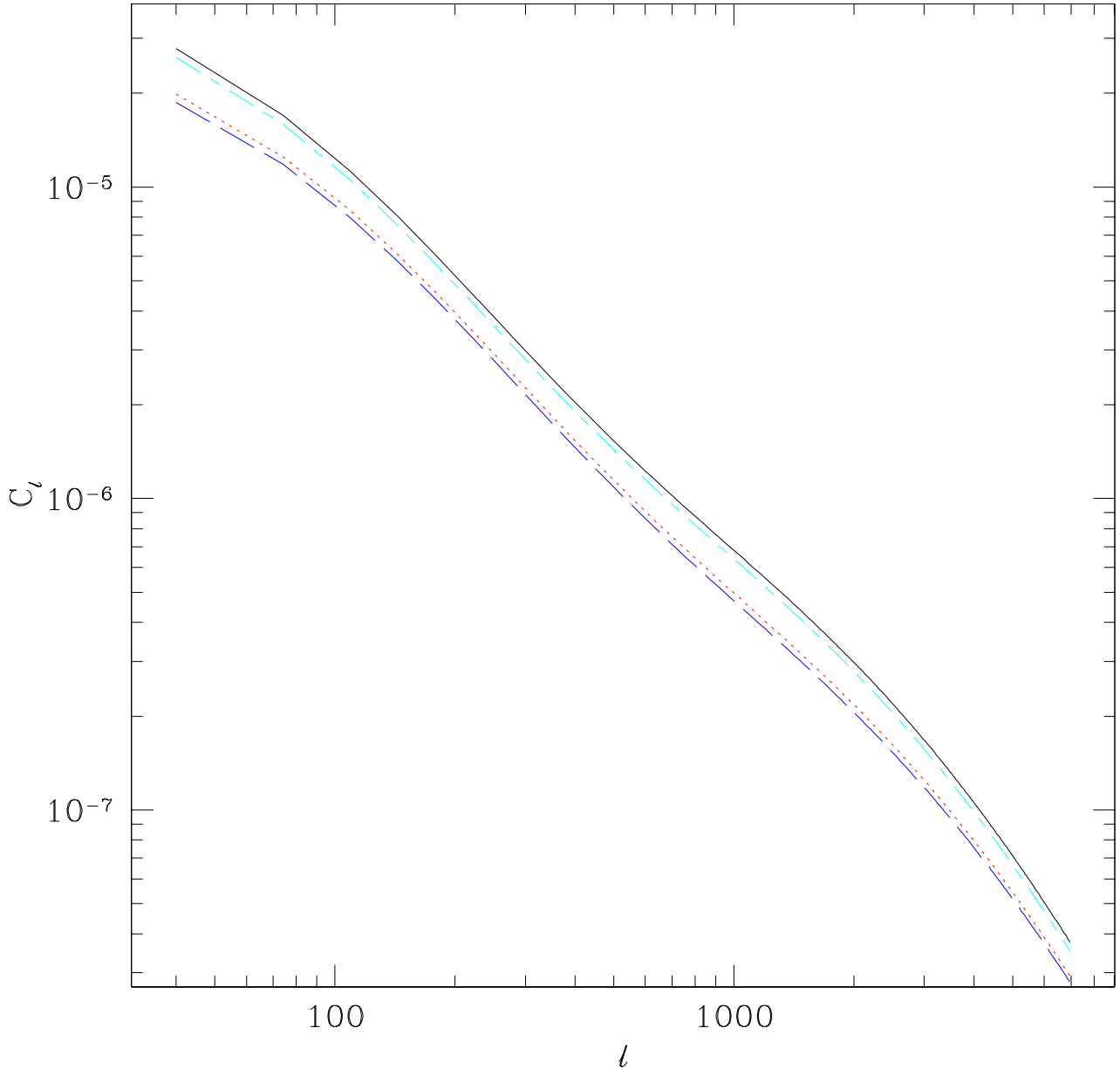


Fig. 6.— The power spectrum for the vanilla model, with  $T_*^{SZ} = 1.2\text{keV}$  (solid line), and that with  $T_*^{SZ} = 2.0\text{keV}$  (dotted line) as might be suggested by X-ray measurements. A higher value,  $T_*^{SZ} = 2.2\text{keV}$  (dashed line) is also shown to give an idea of the change that an expected SZ line of sight projection effect (around 8%) would give. The dot-dashed line fixes  $T_*^{SZ} = 1.2\text{keV}$  but has no evolution in  $f_{gas}$  with mass, i.e.  $f_{gas} = 0.06h^{-3/2}$ , the value for  $M_{vir} = 10^{14}h^{-1}M_{\odot}$ .

into the parameters  $T_*^{SZ} f_{gas}$ . We included the unnoticeable 10% scatter in the  $Y(M)$  relation in all our calculations here.

One might expect that processes such as merging will disrupt the clusters and thus invalidate the assumption of virialization used in some analytic calculations. The most massive clusters have the most recent mergers (as they are generally the most recently formed objects), but these tend to be included automatically in the catalogue as their estimated masses, even if inaccurate, are quite high relative to the mass cut. The selection for the catalogue depends most sensitively on the least massive clusters included, where mergers are relatively rarer. (However, at high redshift the “low mass” clusters are recently formed as they are the most massive collapsed objects at that time, so one might expect some effect from them.) Mergers are automatically included in the cosmological simulations and the scatter in the  $Y - M$  relation is not larger than that expected due to scatter in the  $M - T$  relation (White et al (2002)), leading us to expect that merger induced scatter is relatively small. However, as simulations cannot reproduce cluster properties precisely yet, observational data will be needed to calibrate this effect.

#### 4.2. Cosmic variance, sample variance and shot noise

The last (and crucial effect) we consider here is the inherent statistical measurement error. There are three sources of error for  $C_\ell$  in the absence of any systematic errors: shot noise, cosmic variance and sample variance, which give an overall error

$$\delta C_\ell = \sqrt{\frac{2}{(2\ell + 1)f_{sky}}} \left( C_\ell + \frac{1}{\bar{n}} \right). \quad (34)$$

The factor of  $2\ell + 1$  is due to the  $2\ell + 1$  independent measurements of the power for any  $\ell$ . For small  $\ell$  (large scales) there are very few independent measurements of power in the sky, which is dubbed cosmic variance. Sample variance increases the error as the sky coverage  $f_{sky} \leq 1$  decreases. Shot noise is determined by  $\bar{n}$ , the number density of clusters per steradian.

As the depth of the survey goes up ( $Y_{min}$  decreasing), the power spectrum also decreases, as there are more and more clusters of lower and lower mass, and these are less correlated. However, the shot noise also goes down. On the other hand, as the depth of the survey decreases ( $Y_{min}$  increasing), the power spectrum becomes restricted to higher and higher mass objects and thus goes up. However as these objects are rarer, the shot noise also increases. We can compare these quantities for 3 examples, APEX, SPT, and Planck.

We use the vanilla model and again take  $Y_{min} = 1.7 \times 10^{-5}$  corresponding to a  $5\sigma$  detection for APEX with  $\delta T \sim 10\mu\text{K}$  (at 150 GHz). APEX will survey 100/200 square degrees at two frequencies (214 and 150 GHz, corresponding to 1.4 and 2 mm wavelengths), with 0.75' resolution. For SPT, we expect about 4000 deg<sup>2</sup> and similar sensitivity and resolution. For Planck, we have all sky and will take a rough estimate of  $Y_{min} = 10^{-4}$  (sensitivity/resolution ranging from  $5\mu\text{K}$  at 7.0' to  $50\mu\text{K}$

at  $33.0'$ , depending upon frequency). First we plot the errors due to shot noise, sampling and cosmic variance for the Planck specifications above in figure 4.2. In comparison, those for APEX and SPT are shown in figure 4.2. The vanilla model has the same parameters as earlier (including  $Y_{min} = 1.7 \times 10^{-5}$ , and error bars are shown for 100, 200, and 4000 square degrees, representative areas for data sets expected from APEX and SPT. The largest error bars are for the smallest area. The plot on the upper right has the same observing area, but with a minimum  $Y_{min}$  value of  $10^{-5}$ . This might occur if e.g.  $T_*^{SZ}$  were 2.0 keV rather than 1.2, a reasonable possibility given X-ray measurements and line of sight contamination effects. The sensitivity is directly proportional to  $Y_{min}$ , so “in principle” an experiment can fix  $Y_{min}^2 \times area$  for a given observing time, producing a tradeoff between wide and shallow or narrow and deep. The errors given in equation 34 are shown for the vanilla model correlation function and then compared to other possibilities with fixed observing time. Note this ignores how the efficiency and difficulty of cluster identification changes with  $Y_{min}$ . The bottom two graphs are the vanilla model plotted with a smaller  $Y_{min}$  with error bars corresponding to the 100 and 200 square degree surveys with area up by the factor of 4 or 16 for the left and right graphs respectively. Note that as the sensitivity goes down that the power spectrum and the shot noise go up, as mentioned earlier—only rarer and thus more clustered objects are included. The bin size is the spacing between the error bars, equal in  $\log \ell$ .

These error bars are quite large, but still this measurement contains much useful information. First of all, theory gives us smooth and known functions of  $\ell$ ,  $C_\ell$ , so we can bin  $N_\ell$  nearby values of  $\ell$ , reducing the error roughly by  $1/\sqrt{N_\ell}$ . Secondly, we can go directly to the parameters of interest, of which there are significantly fewer than the number of  $C_\ell$ , and we can combine the  $C_\ell$  measurements as independent measurements of these smaller numbers of parameters, for example  $T_*^{SZ}$ ,  $\sigma_8$ ,  $\Omega_m$  and the bias. For instance, if all the modeling uncertainties were set to zero, APEX could give a  $\sim 10\%$  measurement of  $\sigma_8$  with 200 square degrees. Increasing  $f_{sky}$ , i.e. going to larger area as SPT will do is seen to help significantly.

## 5. Conclusions

Forthcoming SZ surveys such as APEX are expected to observe one or two orders of magnitude more clusters than currently in hand. The angular power spectrum will be an immediate result once clusters have been identified. There still exists uncertainty in theoretical predictions: we examined how those uncertainties affect the cluster power spectrum.

We calculated the angular power spectrum for different reasonable mass functions, biases, mass-temperature normalizations  $T_*^{SZ}$  and gas fractions  $f_{gas}$  and found these changes are comparable to changes due to cosmological parameters of interest such as  $\sigma_8$  within current ranges of interest. We found that the angular power spectrum was insensitive to scatter (less than 1% effect) in the  $Y(M)$  relation when the scatter was taken to be 10% (as recent hydrodynamic simulations suggest).

We also studied the experimental uncertainties which exist even in the absence of systematic

Planck naive errors

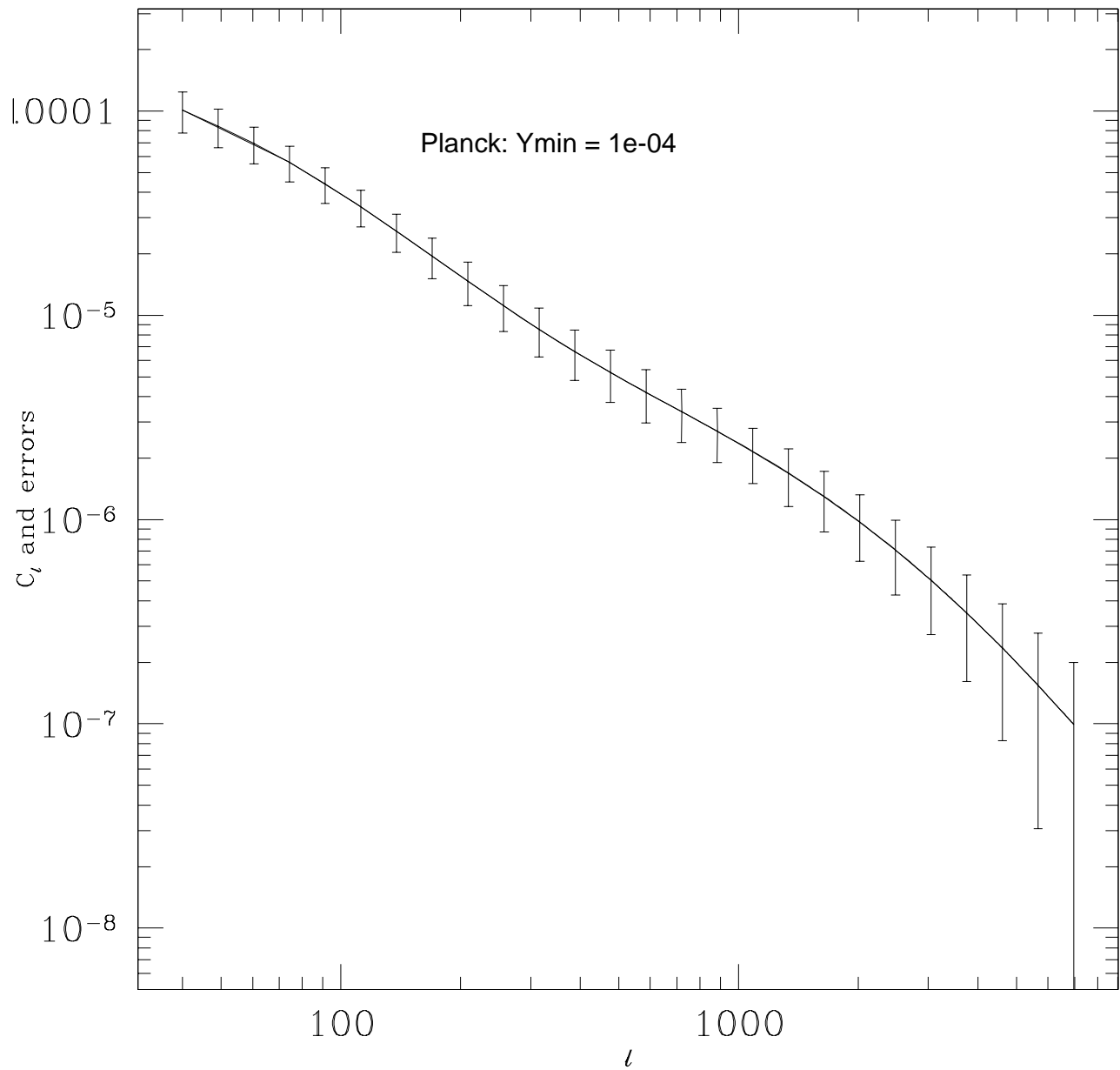


Fig. 7.— The angular power spectrum with errors from shot noise, sampling and cosmic variance error expected from Planck, for a  $Y_{min} = 10^{-4}$ . The bin size is the spacing between the error bars, equal spacing in  $\log l$ . See text for more details.

Area vs. sensitivity

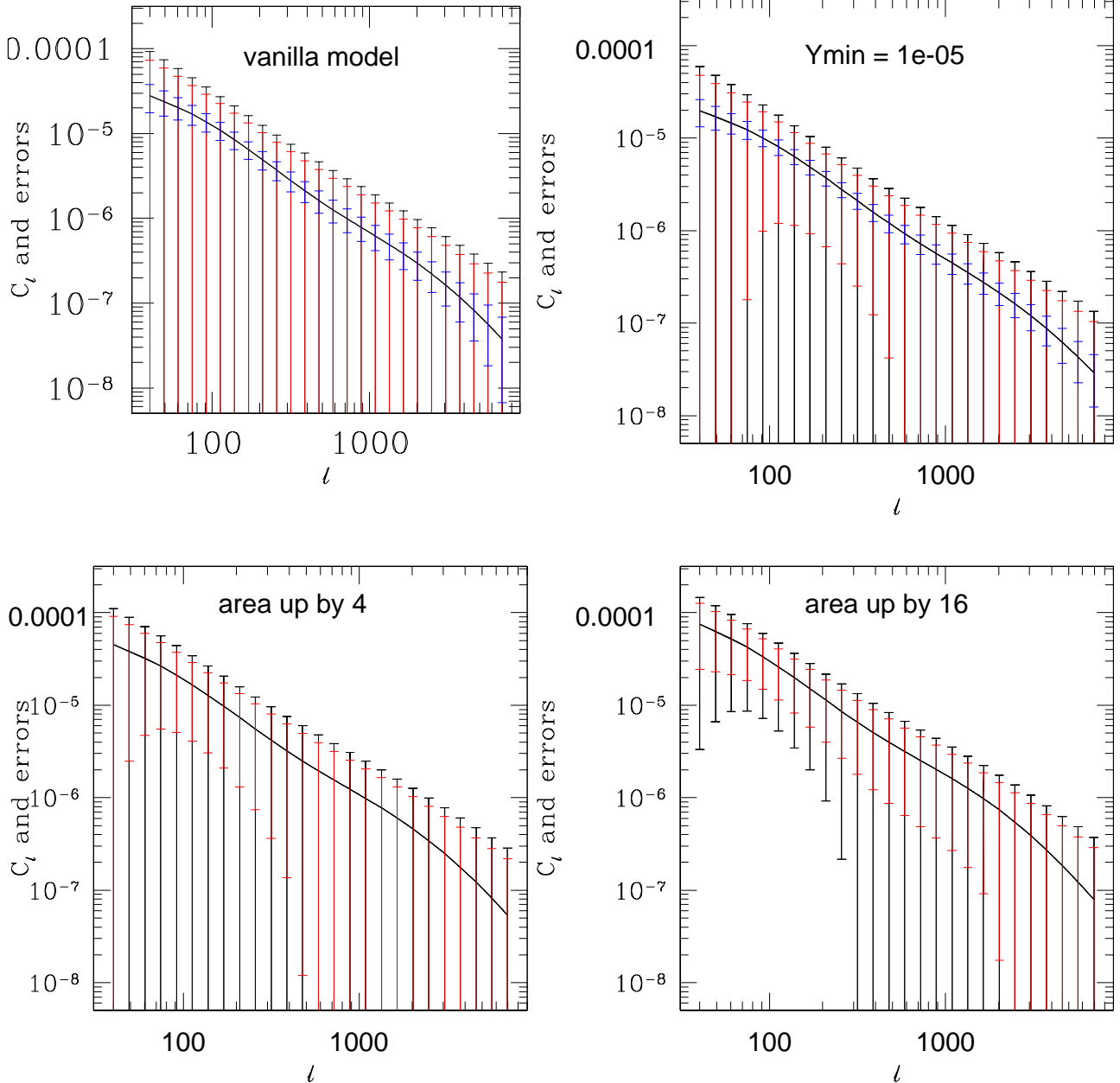


Fig. 8.— The angular power spectrum with errors from shot noise, sampling and cosmic variance error. Error bars are for 100,200 and 4000 square degrees for the top two plots (vanilla model at left,  $Y_{min} = 10^{-5}$  at right), with the largest error bars corresponding to the smallest area. The lower figures correspond to the vanilla model except for the change  $Y_{min} \rightarrow 2Y_{min,vanilla}$  ( $4Y_{min,vanilla}$ ) on the left (right), with the area going up by a factor of 4 (16), relative to the vanilla model at upper left. This naively keeps the observing time fixed. The error bars are equally spaced in  $\log \ell$ . See the text for more details.

uncertainty. We found that in this ideal case, if all the power spectrum measurements were combined, we could still estimate  $\sigma_8$  within 10 % even for a 200 degree APEX survey. In order to really firm up the theory well enough to do such a measurement the mass temperature relation will have to be well calibrated with observations, as will the scatter. Current experiments such as SZA might be able to do this calibration when combined with other measurements for mass, as long as the normalization is not redshift dependent. Simulations with gas are known to have incomplete treatments of physics but can be used as a guide, e.g. to calibrate the effect of projection on the mass temperature relation, which gives a systematic increase of the  $Y(M)$  normalization of about 8%.

We focused on the angular power spectrum alone, though of course complementarity is key to progress. Complementary data will even be provided from survey producing the power spectrum itself. A survey providing an angular power spectrum will also produce number counts per square degree and  $dN/dY$ , number counts as a function of  $Y$ . In addition, the temperature correlation function and perhaps  $dN/dz$  will be available. Various combinations of these quantities have been analyzed in the literature. Mei and Bartlett considered number counts and the angular correlation function, and combined it with the number counts from X-ray, for instance. This is one example of self-calibration (Levine, Schulz & White (2002)); adding the angular power spectrum to other measurements will increase the leverage of all of them. We also would like to note that two preprints appeared simultaneously with ours, Mazzotta et al (2004) and Rasia et al (2004) which further study the difficulties of using X-ray temperatures for galaxy clusters and their cosmological implications.

J.D.C. thanks G. Evrard, E. Reese and W. Hu for discussions and S. Mei for help with comparing with her work and K.K. thanks P. Zhang, W. Hu and J. Weller for useful discussions. We both especially thank M. White for numerous discussions, early collaboration on this project and comments on the draft. This work was supported in part by DOE, NSF grant NSF-AST-0205935 and NASA grant NAG5-10842.

## REFERENCES

- Barbosa, D., Bartlett, J. G., Blanchard, A., Oukbir, J., 1996, *A & A*, 314, 13
- Bardeen, J. M., Bond, J. R., Kaiser, N., Szalay, A. S., 1986, *ApJ* 304, 15
- Bartlett, J.G., Silk, J., 1994, *ApJ*, 423,12
- Bartlett, J.G., 2001, published on arXive as astro-ph/0111211
- Battye, R. & Weller, J., 2003, *Phys Rev D*, 68, 3506
- Birkinshaw, M., 1999, *Phys.Rept.* 310, 97
- Carlstrom, J., Holder, G., Reese, E., 2002, *Ann.Rev.Astron.Astrophys.* 40, 643 [astro-ph/0208192]

- da Silva, A.C., Kay, S.G., Liddle, A.R., Thomas, P.A., 2004, MNRAS 348, 1401
- Diaferio, A., Nusser, A., Yoshida, N., Sunyaev, R., 2003, MNRAS 338, 433
- Eisenstein, D., Hu, W., 1997, ApJ 511, 5
- Ettori, S., Tozzi, P., Borgani, S., Rosati, P., 2004, A & A 417, 13
- Ettori, S., et al, 2004, astro-ph/0407021
- Evrard, A.E., Metzler, C., Navarro, J., 1996, ApJ 469, 494
- Evrard, A.E., et al, 2002, ApJ 573, 7
- Fan, Z.H., Wu, Y.L., 2003, ApJ 598, 713
- Geisbusch, J., Kneissl, R., Hobson, M., astro-ph/0406190
- Hamana, T., Yoshida, N., Suto, Y., Evrard, A.E., 2001, ApJ 561, L143
- Holder, G. P., Mohr, J. J., Carlstrom, J. E., Evrard, A. E., Leitch, E. M., 2000, ApJ, 544, 629
- Holder, G.P., Haiman, Z., Mohr, J.J., 2001, ApJ 560, L111
- Hu, W., & Kravtsov, A., 2003, ApJ, 584, 702
- Huterer, D. & White, M., 2002, ApJ, 578, 2.
- Itoh, N., Kohyama, Y., Nozawa, S., 1998, ApJ, 502, 7
- Jenkins, A., et al, 2001, MNRAS 321, 372
- Kneissl, R., et al., 2001, MNRAS 328, 783
- Knox, L, Holder, G, Church, S, astro-ph/0309643
- Komatsu, E., Kitayama, T., 1999, ApJ 526, L1
- Komatsu, E. & Seljak, U., 2001, MNRAS, 327, 1353
- Komatsu, E. & Seljak, U., 2002, MNRAS, 336, 1256
- Levine, E.S., Schulz, A.E., White, M., 2002, ApJ 577, 569
- Limber, D.N., 1953, ApJ, 117, 134
- Lin, Y.T., Mohr, J.J., Stanford, S.A., 2003, ApJ 591, 749
- Loken, C., et al, 2002, ApJ 579, 571

- Majumdar, S., Mohr, J.J., 2003, ApJ 585, 603
- Majumdar, S., Mohr, J.J., astro-ph/0305341
- Mathiesen, B. & Evrard, A.E., ApJ 546, 100
- Mazzotta, P., et al, 2004, astro-ph/0409650
- Mei, S., Bartlett, J., astro-ph/0407436
- Mei, S., Bartlett, J., 2003, A & A, 410, 767
- Metzler, C., published on arXive as astro-ph/9812295
- Metzler, C., White, M., Loken, C., 2001, ApJ 547, 560
- Mohr, J., Majumdar, S., 2003, AAS 202, 2303
- Moscardini, L.; Bartelmann, M.; Matarrese, S.; Andreani, P., 2002, MNRAS 335, 984
- Navarro, J. F., Frenk, C.S., White, S.D.M., 1997, ApJ 490, 493
- Nozawa, S., et al, 2000, ApJ, 536, 31
- Ota, N., Mitsuda, K., 2004, astro-ph/0407602, A & A to appear.
- Peacock, J.A., Dodds, S.J., 1996, MNRAS 280L, 19
- Pierpaoli E., Borgani, S., Scott, D. & White, M, 2003, MNRAS, 342, 163.
- Press, W., Schechter, P., 1974, ApJ 187, 425
- Kaiser, N., 1984, ApJ 284, L9
- Rasia, E., et al, 2004, astro-ph/0409650
- Rephaeli, Y., 1995, ARA & A 33, 541
- Rephaeli, Y., 1995, ApJ 445, 33
- Sadeh, S., Rephaeli, Y., 2004, New Astronomy, 9, p 373
- Schulz, A.E., White, M., 2003, ApJ 586, 723
- Seljak, U., Warren, M.S., astro-ph/0403698
- Sheth, R., Tormen, G., 1999, MNRAS 308, 119
- Sheth, R., Mo, H.J. Tormen, G., 2001, MNRAS, 323, 1

Smith, R.E. et al, 2003, MNRAS 341, 1311

Sunyaev R. A. & Zel'dovich, 1972, Comm. Astrophys, Space Phys., 4, 173

Sunyaev R. A. & Zel'dovich, Ya. B., 1980, ARA&A, 18, 537

Tegmark, M., et. al, Phys.Rev. D69 (2004) 103501

Wang, S., Khoury, J., Haiman, Z., May, M., 2004, astro-ph/0406331, submitted to Phys Rev D.

White, M., 2001, A & A, 367, 27

White, M., Hernquist, L., Springel, V., 2002, ApJ 579, 16

White, M., Majumdar, S., 2004, ApJ 602, 565